Detection of Hemodynamic Characteristics Before Growth in Growing Cerebral Aneurysms by Analyzing Time-of-Flight Magnetic Resonance Angiography Images Alone: Preliminary Results

Kimura, Hidehito ; Hayashi, Kosuke ; Taniguchi, Masaaki ; Hosoda, Kohkichi ; Fujita, Atsushi ; Seta, Takeshi ; Tomiyama, Akio ; Kohmura,…

(Citation)
World Neurosurgery,122:e1439-e1448

(Issue Date)
2019-02

(Resource Type)
journal article

(Version)
Accepted Manuscript

Title: Detection of Hemodynamic Characteristics Before Growth in Growing Cerebral Aneurysms by Analyzing Time-of-Flight Magnetic Resonance Angiography Images Alone

- Preliminary results -

Authors:

Hidehito Kimura, M.D., Ph.D. [*1]; Kosuke Hayashi, D.Eng. [*2]; Masaaki Taniguchi, M.D., Ph.D. [*1]; Kohkichi Hosoda, M.D., Ph.D. [*3]; Atsushi Fujita, M.D., Ph.D. [*1]; Takeshi Seta, D.Eng. [*4]; Akio Tomiyama, D.Eng. [*2]; Eiji Kohmura, M.D., Ph.D. [*1]

Affiliation:

Department of Neurosurgery, Kobe University Graduate School of Medicine, Kobe, Japan [*1]

Kobe University Graduate School of Engineering, Kobe, Japan [*2]

Department of Neurosurgery, Kobe City Nishi-Kobe Medical Center, Kobe, Japan [*3]

Graduate School of Science and Engineering for Research, University of Toyama [*4]

Corresponding author:

Hidehito Kimura, M.D. Ph.D.

Department of Neurosurgery, Kobe University Graduate School of Medicine

7-5-1, Kusunoki-cho, Chuo-ku, Kobe, 650-0017, JAPAN

Tel.: +81-78-382-5966, Fax: +81-78-382-5979

E-mail: hkimura@med.kobe-u.ac.jp

Key words: cerebral aneurysm, computational fluid dynamics, magnetic resonance angiography, growing, enlargement

ABSTRACT

Objective: Cerebral aneurysm growth often precedes rupture. Definite contributors to aneurysm growth have not been determined even by means of recently developed commercially available computational fluid dynamics (CFD) software. We developed an original CFD tool that can analyze data from time-of-flight magnetic resonance angiography (TOF-MRA) prior to growth in the growing aneurysms and investigate possible factors for aneurysm growth in the near future.

Methods: We retrospectively reviewed unruptured aneurysms that were treated at our institute because of aneurysm growth (growing group) between April 2013 and March 2017. Stable aneurysms that had demonstrated no growth for more than five years were selected (stable group). TOF-MRA data of these aneurysms were retrospectively converted to three-dimensional vessel geometric data; three hemodynamic indices including streamline, wall shear stress (WSS), and oscillatory shear index were calculated by our original CFD tool using the lattice Boltzmann method to quantitatively compare the two groups.

Results: Six growing aneurysms and 6 stable aneurysms were analyzed. Of the 6 growing aneurysms, WSS on the focal aneurysmal sac increased temporally in the vicinity of the constant low WSS area at the peak systolic phase. By contrast, WSS did not increase during any part of the

cardiac cycle in three of the six stable aneurysms. The peak values of WSS were significantly different between the two groups.

Conclusion: A focal increase in WSS in the peak systolic phase may be a risk factor for aneurysm enlargement in the near future.

INTRODUCTION

Unruptured intracranial aneurysms are mostly asymptomatic. A few per year enlarge and later rupture, causing subarachnoid hemorrhage (SAH)[1, 2]. Despite substantial improvements in clinical care of these patients, the morbidity and mortality of aneurysmal SAH remain too high to be ignored, and some patients suffer devastating outcomes[3]. Therefore, an objective assessment tool that would reliably identify patients at risk for aneurysm growth and rupture would be beneficial, enabling preventative interventions, such as endovascular coiling and microsurgical clipping[2].

Some clinical and morphological factors, including patient sex and aneurysm size and location, may help predicting the rupture risk of incidentally detected aneurysms[1, 4, 5]. However, the trustworthiness of patient specific factors in prediction of aneurysm rupture remains unclear.

Recent advances in computational fluid dynamics (CFD) have enabled the study of hemodynamics in realistic aneurysm geometries[6]. Among hemodynamic parameters, wall shear stress (WSS) was reported to be a key parameter in the development, growth, and rupture of intracranial aneurysms[7, 8]. Despite a variety of efforts to study this matter, researches on its relationship with the risk of aneurysm growth and rupture showed conflicting results: in some studies this risk was associated with high WSS, while in others with low WSS, in an individual

aneurysm [9-11].

In order to clarify hemodynamic features contributing to aneurysm growth and rupture, a retrospective review and analysis of the original cerebral aneurysm data before growth or rupture should be ideally conducted, in order to determine the actual factors causing aneurysm growth and rupture[12]. Unfortunately, little data on aneurysms hemodynamic status before growth or rupture are available after they grow or rupture, which made this retrospective analysis almost impossible[13].

Growing, unruptured intracranial aneurysms have often been detected by time-of-flight-magnetic resonance angiography (TOF-MRA), a widely used magnetic resonance imaging (MRI) sequence used to screen for intracranial abnormalities owing to its non-invasive nature[14]. However, no study on CFD analysis of TOF-MRA data has been published, because commercially available CFD software could compute the data from rotational angiography or three-dimensional (3D) computed tomography angiography (CTA), but not from TOF-MRA.

Therefore, we launched and developed a new in-house CFD tool using only TOF-MRA images for analyzing the fluid dynamics of cerebral aneurysms, and named it “AN2WER”, abbreviated from “Aneurysms Answer.”

The objective of the present study was to identify possible factors predicting impending

aneurysm growth using our original CFD tool, AN2WER, by analyzing the flow-dynamic features of growing aneurysms using TOF-MRA data collected before growth and comparing quantitatively obtained data to those of stable aneurysms.

METHODS

Patient population (Table 1)

This was a retrospective study. Between April 2013 and March 2017, a total of 526 patients were referred to our institute with the diagnosis of unruptured intracranial aneurysms, and most of these patients were followed-up with TOF-MRA annually. Among them, 9 aneurysms were found to have grown without symptoms. We enrolled six of those patients as the growing group, according to the following inclusion criteria: 1) saccular aneurysm; 2) age between 20 and 90 years; 3) enlargement by 1.0 mm or more in the longest line originating from the centroid of the neck surface compared to previous TOF-MRA images; 4) at least a six-month interval from the initial images; and 5) available TOF-MRA data on prior-to-growth aneurysm status.

In the same patient population, we searched for stable aneurysms in patients who met the following inclusion criteria: 1) saccular aneurysm; 2) age between 20 and 90 years; 3) no change in the size or shape of the aneurysm for at least five years; and 4) available initial TOF-MRA data. We randomly selected six stable aneurysms in five patients.

MRI findings of these patients were certified by two radiologists.

Our institutional review board approved this study, and written informed consent was obtained from all patients.

TOF-MRA condition

The three-dimensional TOF-MRA images were acquired on 1.5T or 3.0T MRI scanners (Achieva 1.5T Nova Dual, Philips; Achieva 3.0T TX Quasar Dual, Philips; Ingenia 3.0T R5.1.7, Philips; Taitan 3T, Toshiba Medical Systems). The imaging parameters for 3D TOF-MRA on these four scanners were as follows: field of view: 207 mm×230 mm, 184 mm×230 mm, 184 mm×230 mm and 200 mm×192 mm; matrix: 140×400, 243×608, 243×608 and 208×272; and repetition time/echo time: 25 ms/6.91 ms, 25 ms/3.45 ms, 25 ms/3.45 ms and 21 ms/3.4 ms. The slice thickness was 1.1 mm for the first three scanners and 1.0 mm for the Taitan 3T. The parameters

for each scanner were manufacturer-installed settings and were not customized ones.

CFD analysis with AN2WER

Blood flows were simulated using the lattice Boltzmann method (LBM), which gives the time evolution of the velocity distribution functions, f_i, of the ith group of fluid particles by accounting for particle advection and collision. LBM solves the following lattice Boltzmann equation for the ith discrete velocity distribution function f_i [15]:

$$f_i(\boldsymbol{x} + \boldsymbol{c}_i\Delta t, t + \Delta t) = f_i(\boldsymbol{x}, t) + \Omega_i$$

where $\boldsymbol{x}$ is the Cartesian coordinate, $\Delta\boldsymbol{x}$ is the grid size, t is the time, Δt is the time step size, $\boldsymbol{c}_i$ is the discrete velocity of the ith distribution function, and Ω is the collision operator, which is modeled using the single relaxation time approximation:

$$\Omega_i = -\frac{f_i(x,t) - f_i^{eq}(x,t)}{\tau}$$

where the superscript eq denotes the equilibrium value, and τ is the relaxation time[15]. The macroscopic variables (density and velocity) were obtained by taking moments of f_i. Nineteen discrete velocity components (the D3Q19 discrete velocity model) were used for the 3D simulations.

Cartesian computational grids were used in the lattice Boltzmann simulations, whereas the curved boundaries of blood vessels reconstructed from the aneurysmal geometrical models were accounted for by applying the bounce-back boundary condition. For the reconstruction of the geometrical model, TOF-MR data obtained at 1.5T or 3.0T (Fig. 1A) were imported to OsiriX (Pixmeo, Bernex, Switzerland), which enabled us to obtain a geometrical model represented by a set of triangular elements (stereolithographic (STL) mesh data) (Figs. 1B and C). The interpolated bounce-back rule for curved boundaries [16] was used to address the complicated channel structure of blood vessels. The distance from the boundary was required at each grid point under this bounce-back rule; therefore, the signed-distance function was reconstructed from the STL mesh (Fig. 1D)[17]. LBM was suitable for parallel computing owing to the locality of the collision process. The General-Purpose Computing on Graphics Processing Units was employed for parallel computing.

The Reynolds number, *Re*, and the Womersley number, *Wo*, were set to typical values in cerebral arteries, i.e., $Re = 200$ and $Wo = 2.5$, [18], where $Re = U_0 D/\nu$, $Wo = \omega D^2/4\nu$, U_0 is the mean inlet velocity, D is the circle-area-equivalent inlet diameter, ν is the kinematic viscosity, and ω is the angular frequency of pulsatile blood flow. The unsteady flow rate of blood was given as a simple

function of time to model typical pulsatile flow, (see Fig. 1E, in which U is the time-dependent inlet velocity and T is the period of cardiac cycle)[19]. The non-Newtonian characteristics of blood were accounted for by means of the Casson model for viscous stress [20]. It should be noted, however, that the Bingham number, Bi, in cerebral arteries is typically small, e.g., 0.1, such that the non-Newtonian effect on blood flow is expected to be small. The Bingham number is defined as $Bi = \tau_0 D/\eta\, U_0$, where τ_0 is the yield stress and η is the viscosity.

With this tool, named "AN2WER", we could perform patient-specific pulsatile blood flow simulations for the arterial geometry during the cardiac phase and calculated three hemodynamic indices: (a) stream line, (b) WSS, (c) oscillatory shear index (OSI). It should be noted that in the following sections, the viscous shear stresses in evaluation of WSS and OSI were scaled by $\rho U_0^2/2$, which is the time-averaged dynamic pressure in a parent artery, to clearly show how large the shear stresses in cerebral aneurysms are compared with the kinetic energy of the blood flow in the parent arteries.

Accuracy of AN2WER compared to that of the conventional tool

To confirm the accuracy of AN2WER, we calculated WSS at the sac and parent artery of each

aneurysm, one by using CTA data after growth with commercially available CFD software Hemoscope Ver. 1.5 (EBM corp., Tokyo, Japan), and another by using TOF-MRA data after growth with AN2WER. These results were compared qualitatively regarding WSS distribution.

Detection of factors contributing to aneurysm growth

Using AN2WER, we performed CFD analysis using TOF-MRA data of the growing and the stable group and calculated streamline, WSS, and OSI. These results were assessed qualitatively by comparing the distribution of color maps between the groups. If differences could be detected in two parameters, including WSS and OSI, quantitative evaluations were performed as described above.

Statistical analysis

Continuous variables were presented as means and standard deviations, and categorical variables were presented as percentages. Welch's *t*-test was used to compare continuous variables and proportions. Fisher's exact test was used to analyze differences in categorical factors. All statistical analyses were performed using EZR (Saitama Medical Center, Jichi Medical University,

Saitama, Japan), a graphical user interface for R 3.0.1 (R Foundation for Statistical Computing, Vienna, Austria). A p value <0.05 was considered statistically significant.

RESULTS

Patient characteristics

In the growing group, there were five women and one man, with a mean age of 63.0 years (range, 45-80 years). Two internal carotid artery (ICA) aneurysms, two anterior communicating artery (Acom) aneurysms, and one aneurysm each of the middle cerebral artery (MCA) and distal anterior cerebral artery were included. The initial maximum aneurysm diameter ranged from 2.5 to 8.5 mm (mean, 4.1 ± 2.0 mm). Aneurysms enlarged to sizes ranging from 4.5 mm to 11.8 mm (mean, 6.1± 2.6 mm) over a clinical observation period lasting an average of 44.7 months (Table 1).

In the stable group, by contrast, there were five women and one man with a mean age of 76.3 years (range, 60 to 105 years). Three ICA aneurysms and one aneurysm each of the Acom, the MCA, and the junction of the vertebral artery and the posterior inferior cerebellar artery were included. The maximum aneurysm diameter ranged from 4.1 to 7.0 mm (mean, 5.5 mm ± 1.0 mm).

Aneurysms were stable over an observation period lasting an average of 76.3 months (Table 1). No significant differences were found between the two groups in terms of age, male/female ratio, follow-up period, or initial aneurysm size.

Illustrative case (Fig. 2)

A 69-year-old woman was incidentally found to have an unruptured right IC-posterior communicating artery aneurysm that was 8.5 mm in maximum diameter. The aneurysm gradually enlarged to 11.8 mm after eleven months of clinical observation, and the patient underwent surgical clipping to prevent its rupture.

CFD analysis was retrospectively performed with AN2WER using TOF-MRA images acquired at the initial examination and after aneurysm enlargement. Imaging and analysis of flow dynamics including streamline, WSS, and OSI were successfully obtained; these imaging data included dynamic WSS videos spanning one complete cardiac cycle (Fig. 2). In the peak systolic phase, WSS was increased at the focal aneurysmal sac where the aneurysm would enlarge in the future (Fig. 2).

Accuracy of AN2WER compared to that of the conventional tool

Among a total of six growing aneurysms, four patients underwent surgical interventions, including three microsurgical clippings and one endovascular coiling at our institute. The three patients who underwent clipping had both 3D-CTA and TOF-MRA data recorded after growth. We tried to use TOF-MRA data for analysis with Hemoscope Ver. 1.5. However, it could not read the TOF-MRA data as expected, and the data could not be analyzed. Therefore, we used 3D-CTA data recorded after growth to conduct hemodynamic analysis with Hemoscope Ver. 1.5, and successfully calculated WSS. In addition, we applied AN2WER to TOF-MRA data recorded after growth to calculate WSS and compared the results of hemodynamic analysis with Hemoscope Ver. 1.5 (Fig. 3). The distribution of high and low WSS in all three aneurysm sacs and around the aneurysm necks calculated with Hemoscope Ver. 1.5 was quite similar to the results obtained with AN2WER (Fig. 3).

Detection of factors contributing to aneurysm growth

Imaging and analysis of flow dynamics were successfully obtained in all cases (Figs. 2, 4, 5). In all six growing aneurysms, marked increases in WSS were demonstrated at the focal areas on

the aneurysm sacs in the vicinity of constant low WSS areas, at the peak systolic phase before aneurysm growth. The values for cases 1 to 6 were 0.074, 0.106, 0.37, 0.13, 0.26, and 0.25, respectively (Fig. 4). By contrast, in three of six stable aneurysms (Fig. 5; cases 1, 3, 5), no apparent increase in WSS was recognized at the aneurysm sac. The values were 0.0066, 0.045 and 0.0019, respectively. In the remaining three stable aneurysms (Fig. 5; cases 2, 4, 6), a focal, generally mild, increase in WSS was demonstrated in the peak systolic phase, and the values were 0.487, 0.073 and 0.117, respectively.

The peak WSS values of the growing aneurysms during the peak systolic phase had a median of 0.190 (interquartile range, 0.112 to 0.258), and those of stable aneurysms had a median of 0.045 (interquartile range, 0.007 to 0.073) (Fig. 6). The peak WSS tended to be higher in growing aneurysms than in the stable aneurysms. Among the stable aneurysms, case 2, a paraclinoid aneurysm, had an outlier value of 0.487, much higher than the upper whisker, and was excluded. Finally, these differences were statistically significant ($p < 0.05$) (Fig. 6).

Neither the geometric flow streamline nor the OSI showed any specific differences between growing and stable aneurysms.

DISCUSSION

We successfully performed CFD analysis using TOF-MRA images alone using our newly developed CFD tool AN2WER. This is the first report on successful CFD analysis using TOF-MRI images alone for cerebral aneurysms. The tool enabled us to conduct a retrospective analysis of original aneurysm data before growth and to demonstrate the actual hemodynamic situation before aneurysm growth in growing aneurysms. We found that transient, focal high WSS areas of aneurysm sacs in the vicinity of stable low WSS areas at the peak systolic phase was associated with future aneurysm growth.

Significance of CFD analysis from TOF-MRA

TOF-MRA might not provide accurate geometric information[21], and its data have been assumed to be unsuitable for CFD analysis. However, TOF-MRA is a less invasive examination method that can be performed without injection of contrast medium or exposure to radiation. Therefore, it is familiar and popular as a follow-up tool for incidental detection of aneurysms and has often reveled growing unruptured intracranial aneurysms. If the data of TOF-MRA could be used for CFD analysis, we could analyze the original flow conditions prior to aneurysm growth.

However, commercially available software programs could use only high-resolution images from rotational angiography or CTA, but not from TOF-MRA, and these data are used to solve Navier-Stokes equations by means of finite element techniques or finite volume techniques, and to calculate numerical hemodynamic indices, including WSS and OSI. The resolution of TOF-MRA seemed to have been inferior to that of the former two facilities, possibly explaining why commercially available software could not solve the data of TOF-MRA accurately. Therefore, no reports of CFD analysis for unruptured cerebral aneurysms using data from TOF-MRA alone are currently available. Actually, in the present study, we tried to solve the data of TOF-MRA in three cases using Hemoscope and failed to do so.

Phase-contrast MRI (PC-MRI) is known to be a non-invasive sequence that is and able to reveal intracranial arteries and cerebral aneurysms as well as TOF-MRA, which can be performed without contrast medium or exposure to radiation[14]. Therefore, there have been a few reports of CFD analysis using PC-MRI[14, 22, 23]. However, PC-MRI is an unusual sequence because of its time-consuming matter, and it has not been adopted for medical check-up screening for cerebral aneurysms. TOF-MRA has been a unique and widely used sequence for screening of intracranial

cerebral aneurysms because of its less-invasive, time-saving character and because the geometrical information provided by this technique is better than that of PC-MRI.

In this study, we first successfully used TOF-MRA alone in CFD analysis by solving LBM as an alternative to solving Navier-Stokes equations. This method is not yet popular for computational hemodynamics and no commercially-available software that uses the lattice Boltzmann equation to analyze hemodynamics of cerebral aneurysms has been established. Only a few authors have reported their experiences with hemodynamic simulation for cerebral aneurysms by applying the lattice Boltzmann equation using their in-house code[24, 25]. Their conclusions were that LBM could be considered an alternative solver for computational hemodynamics of cerebral aneurysms. Thus, we tried to solve the data of TOF-MRA with LBM, and we succeeded. LBM appears to be a suitable solver for TOF-MRA data.

It remains uncertain why the LBM could solve the data of TOF-MRA. When operating the Hemoscope, we needed to accurately trace and register the centerline of the target vessels. With the rough images of TOF-MRA, it appeared that Hemoscope could not recognize the centerline precisely. However, with our tool using LBM, we did not need to trace the centerline of the parent arteries. The rough surface of vessels was smoothed appropriately enough with Osirix to to solved.

Although no more than three cases were compared qualitatively, we found that the distribution of WSS on the aneurysm sacs calculated by our in-house CFD analysis tool using LBM was quite similar to that obtained by commercially available software using Navier-Stokes equations. Our tool might become an alternative method for CFD analysis of cerebral aneurysms with the great advantage that it can analyze TOF-MRA data.

Prediction of aneurysm growth

Few previous studies analyzed the hemodynamics of growing intracranial aneurysms using longitudinal data, but they reported confusing and inconsistent results[9, 12, 26, 27]. Boussel et al. analyzed hemodynamics in seven growing aneurysms and proposed that the growth occurred at regions of abnormally low WSS[9]. Similarly, Brinjikji et al found that growing aneurysms had larger areas under low WSS than did stable aneurysms[26]. By contrast, Sforza et al. suggested that concentrated high WSS could represent the characteristics of hemodynamic environments that promoted aneurysmal growth[28]. Others concluded that the growing region could be exposed to either high WSS or low WSS[27].

Possible reasons for these inconsistent results might include varying methods of evaluation[29].

For example, Boussel et al. evaluated WSS as the time average, not the maximum, during the cardiac cycle and reported that time-averaged WSS was significantly lower in the area of the aneurysm growth[9]. Brinjikji et al. reported that growing aneurysms had significantly greater area under low WSS than did stable aneurysms; their study did not focus on lesions with high WSS[26].

We presumed that the problem was not the extent of low WSS. We focused on the time-dependent increase in WSS on the aneurysm sac during the cardiac cycle. We found that aneurysms with even small areas of high WSS that were recognized only at the peak systolic phase could grow in the future, as in cases 2, 4 and 6 (Fig. 4). If WSS was calculated as a time average, this small area of temporally high WSS could disappear into the wide area of low WSS, and we would not detect its existence. In fact, Brinjikji et al. reported similar cases, with a wide area of low WSS and focal high WSS on the aneurysm sac that grew during the 1-year follow-up[26]. However, this focal high WSS was not the focus of their study. Not only a wide area of low WSS but also an area of temporarily high WSS, though small, might be necessary for aneurysm growth. In this study, we found that the difference in this temporal increase of WSS was statistically significant between growing and stable aneurysms.

Recently, Sforza et al. reported that growing aneurysms tended to have complex intrasaccular

flow patterns that induced non-uniform WSS distributions with areas of concentrated high WSS and large areas of low WSS. Their findings were in agreement with our findings[28].

Although aneurysm growth has been found to be highly related to aneurysm rupture, the most important task in the management of unruptured aneurysms is to predict ruptures before they occur as opposed to merely when they grow. This problem is yet to be solved, and the "high WSS or low WSS" issue remains confusing in the literature. In recent published articles, other hemodynamic parameters including WSS gradient, OSI, and aneurysm formation indicator, had been investigated to clarify cerebral aneurysm condition, but had not been fully succeeded[29, 30, 31]. Our novel CFD tool AN2WER appeared to analyze TOF-MRA data accurately. Using this technique, we will be able to measure these hemodynamic parameters by analyzing TOF-MRA data prior to aneurysm rupture in ruptured aneurysms, and expect to be able to propose risk factors for aneurysm rupture from a new viewpoint.

Limitations

The current study has some limitations. First, as with all CFD studies on cerebral aneurysms, several assumptions were made. Inflow profiles were not patient-specific and were taken from a

cohort of healthy patients. The vessel wall was assumed to be rigid[32, 33]. However, previous investigators indicated that these are second-order issues with only minimal effects on flow dynamics, whereas the most important factor is the actual vessel geometry[34, 35].

Second, the sample size was too small to establish an original CFD tool or to detect undeniable factors. We realize that our results are preliminary. We compared solved results between AN2WER and Hemoscope in no more than three cases. With this limited comparison, a potential error or inaccuracy could not be denied sufficiently in smoothing the anatomical data. We should investigate more cases to clarify the accuracy of AN2WER. Moreover, in the detection of factors contributing to aneurysms growth, we compared only six aneurysms between the two groups. Although we obtained a statistically significant result, we are going to perform further analysis on more cases accumulated retrospectively and to perform prospective observation of analyzed aneurysms to obtain definite results. The problem with this investigation is not only that we have a few chances to encounter the growing aneurysm in the outpatient department, but also its complicated procedure and time-consuming analysis. In order to resolve these matters, we will perform a multicenter study to accumulate more cases, improve AN2WER, and facilitate and save time in analysis. Furthermore, in terms of small sample size, Case 2 in the stable aneurysm group,

which was the only case harboring a paraclinoid aneurysm, was excluded for having an outlier value. We presumed this outlier value might derive from its anatomical characteristics, i.e., the parent artery that was fixed tightly to the skull base dura and the aneurysm itself was fixed, possibly only partially, to a bony structure such as the anterior clinoid process, possibly producing unique hemodynamic characters. To resolve these matters, we should perform subgroup analysis based on its location after accumulating a sufficient number of cases and re-consider the significance of this outlier value.

Third, from the point of view of the resolution of TOF-MRA, the image resolution of 1.5T TOF-MRA was inferior to that of 3.0T TOF-MRA. Fortunately, we did not encounter any problems in solving the images even using 1.5T TOF-MRA. We should precisely discriminate these two different conditions because the results from two images might give potential differences that were not detected in the present study.

Finally, we could not determine the relationship between the areas of temporally increased WSS on the aneurysm dome and the actually enlarged regions because we could not detect them by TOF-MRA images before and after aneurysm growth. Further analyses applied to more cases with AN2WER using the high-resolution 3T-MRI may clarify this matter. In addition, we did not

validate the results histopathologically by comparing the aneurysm specimens taken from the actual surgery. Combined with histopathological analyses, the actual mechanisms contributing to aneurysm growth could be clarified.

CONCLUSION

Our newly developed CFD method enabled us to perform CFD analysis using TOF-MRA images alone, a task that cannot yet be performed with commercially available software. We conducted a retrospective analysis of the original aneurysm data before growth and demonstrated the actual hemodynamic situation in growing aneurysms.

Although further analysis of accumulated cases is needed to clarify obtained results, our present preliminary study demonstrated that transient, focal high WSS areas of the aneurysm sac at the peak systolic phase in the vicinity of constant low WSS areas might be related to future aneurysm growth.

ACKNOWLEDGEMENT

We thank Mr. Susumu Osaki and Mr. Noriyuki Negi for technical assistance in CFD analysis with our tool AN2WER and Hemoscope Ver. 1.5, respectively.

FUNDING

The authors report no conflict of interest concerning the materials or methods used in this study or the findings specified in this paper.

REFERENCES

1. Morita A, Fujiwara S, Hashi K, Ohtsu H, Kirino T. Risk of rupture associated with intact cerebral aneurysms in the Japanese population: a systematic review of the literature from Japan. *J Neurosurg*. 2005;102(4):601-606. doi:10.3171/jns.2005.102.4.0601.

2. Wiebers DO, Whisnant JP, Huston J, et al. Unruptured intracranial aneurysms: natural history, clinical outcome, and risks of surgical and endovascular treatment. *Lancet (London, England)*. 2003;362(9378):103-110. http://www.ncbi.nlm.nih.gov/pubmed/12867109. Accessed October 1, 2017.

3. Connolly ES, Rabinstein AA, Carhuapoma JR, et al. Guidelines for the Management of Aneurysmal Subarachnoid Hemorrhage. *Stroke*. 2012;43(6). http://stroke.ahajournals.org/content/43/6/1711.long. Accessed August 4, 2017.

4. Shiue I, Arima H, Hankey GJ, Anderson CS. Location and size of ruptured intracranial aneurysm and serious clinical outcomes early after subarachnoid hemorrhage: a population-based study in Australasia. *Cerebrovasc Dis*. 2011;31(6):573-579. doi:10.1159/000324938.

5. Wermer MJH, van der Schaaf IC, Algra A, Rinkel GJE. Risk of rupture of unruptured intracranial aneurysms in relation to patient and aneurysm characteristics: an updated meta-

analysis. *Stroke*. 2007;38(4):1404-1410. doi:10.1161/01.STR.0000260955.51401.cd.

6. Steinman DA. Image-Based Computational Fluid Dynamics Modeling in Realistic Arterial Geometries. *Ann Biomed Eng*. 2002;30(4):483-497. doi:10.1114/1.1467679.

7. Imbesi SG, Kerber CW. Analysis of Slipstream Flow in Two Ruptured Intracranial Cerebral Aneurysms . http://www.ajnr.org/content/20/9/1703/F2.expansion.html. Accessed August 25, 2015.

8. Mantha A, Karmonik C, Benndorf G, Strother C, Metcalfe R. Hemodynamics in a cerebral artery before and after the formation of an aneurysm. *AJNR Am J Neuroradiol*. 2006;27(5):1113-1118. http://www.ncbi.nlm.nih.gov/pubmed/16687554. Accessed August 25, 2015.

9. Boussel L, Rayz V, Mcculloch C, et al. Aneurysm Growth Occurs at Region of Low Wall Shear Stress Patient-Specific Correlation of Hemodynamics and Growth in a Longitudinal Study. doi:10.1161/STROKEAHA.108.521617.

10. Hashimoto T, Meng H, Young WL. Intracranial aneurysms: links among inflammation, hemodynamics and vascular remodeling. *Neurol Res*. 2006;28(4):372-380. doi:10.1179/016164106X14973.

11. Meng H, Wang Z, Hoi Y, et al. Complex Hemodynamics at the Apex of an Arterial Bifurcation Induces Vascular Remodeling Resembling Cerebral Aneurysm Initiation. *Stroke*. 2007;38(6):1924-1931. doi:10.1161/STROKEAHA.106.481234.

12. Xiang J, Tutino VM, Snyder K V., Meng H. CFD: Computational Fluid Dynamics or Confounding Factor Dissemination? The Role of Hemodynamics in Intracranial Aneurysm Rupture Risk Assessment. *Am J Neuroradiol*. 2014;35(10):1849-1857. doi:10.3174/ajnr.A3710.

13. Le W-J, Zhu Y-Q, Li M-H, et al. New method for retrospective study of hemodynamic changes before and after aneurysm formation in patients with ruptured or unruptured aneurysms. *BMC Neurol*. 2013;13:166. doi:10.1186/1471-2377-13-166.

14. Naito T, Miyachi S, Matsubara N, et al. Magnetic resonance fluid dynamics for intracranial aneurysms—comparison with computed fluid dynamics. *Acta Neurochir (Wien)*. 2012;154(6):993-1001. doi:10.1007/s00701-012-1305-5.

15. Chen S, Doolen GD. LATTICE BOLTZMANN METHOD FOR FLUID FLOWS. *Annu Rev Fluid Mech*. 1998;30(1):329-364. doi:10.1146/annurev.fluid.30.1.329.

16. Aidun CK, Clausen JR. Lattice-Boltzmann Method for Complex Flows. *Annu Rev Fluid*

Mech. 2010;42(1):439-472. doi:10.1146/annurev-fluid-121108-145519.

17. Hayashi, K., Sou, A., Tomiyama A. A volume tracking method based on non-uniform subcells and continuum surface force model using a local level set function. *Comput Fluid Dyn J*. 15(2):225-232. https://www.researchgate.net/publication/285761857_A_volume_tracking_method_based_on_non-uniform_subcells_and_continuum_surface_force_model_using_a_local_level_set_function. Accessed September 22, 2017.

18. Yamaguchi T. Multi-Scale Computational Biomechanics of Arterial Diseases. http://www.nanobme.org/en/annals/articles07/2007_en_005-014.pdf. Accessed September 22, 2017.

19. Funazaki K-I, Higashi M, Yamada K, Taniguchi H, Tomura N. Flow-Structure Coupled Analysis of Cerebrovascular Artery with an Aneurysm of Realistic Geometry. https://www.jstage.jst.go.jp/article/kikaib1979/73/731/73_731_1472/_pdf. Accessed September 22, 2017.

20. Ohta, M., Nakamura, T., Yoshida, Y., Matsukuma Y. Lattice Boltzmann simulations of

viscoplastic fluid flows through complex flow channels. *J Nonnewton Fluid Mech*. 2011;166(7-8):404-412. doi:10.1016/J.JNNFM.2011.01.011.

21. Isoda H, Ohkura Y, Kosugi T, et al. Comparison of hemodynamics of intracranial aneurysms between MR fluid dynamics using 3D cine phase-contrast MRI and MR-based computational fluid dynamics. doi:10.1007/s00234-009-0634-4.

22. Isoda H, Ohkura Y, Kosugi T, et al. Comparison of hemodynamics of intracranial aneurysms between MR fluid dynamics using 3D cine phase-contrast MRI and MR-based computational fluid dynamics. *Neuroradiology*. 2010;52(10):913-920. doi:10.1007/s00234-009-0634-4.

23. Isoda H, Ohkura Y, Kosugi T, et al. In vivo hemodynamic analysis of intracranial aneurysms obtained by magnetic resonance fluid dynamics (MRFD) based on time-resolved three-dimensional phase-contrast MRI. *Neuroradiology*. 2010;52(10):921-928. doi:10.1007/s00234-009-0635-3.

24. Abas A, Mokhtar NH, Ishak MHH, Abdullah MZ, Ho Tian A. Lattice Boltzmann Model of 3D Multiphase Flow in Artery Bifurcation Aneurysm Problem. *Comput Math Methods Med*. 2016;2016:6143126. doi:10.1155/2016/6143126.

25. Weichert F, Walczak L, Fisseler D, et al. Simulation of Intra-Aneurysmal Blood Flow by Different Numerical Methods. *Comput Math Methods Med*. 2013;2013:1-10. doi:10.1155/2013/527654.

26. Brinjikji W, Chung BJ, Jimenez C, Putman C, Kallmes DF, Cebral JR. Hemodynamic differences between unstable and stable unruptured aneurysms independent of size and location: a pilot study. *J Neurointerv Surg*. April 2016:neurintsurg-2016-012327. doi:10.1136/neurintsurg-2016-012327.

27. Sugiyama SI, Meng H, Funamoto K, et al. Hemodynamic analysis of growing intracranial aneurysms arising from a posterior inferior cerebellar artery. *World Neurosurg*. 2012;78(5):462-468. doi:10.1016/j.wneu.2011.09.023.

28. Sforza DM, Kono K, Tateshima S, Viñuela F, Putman C, Cebral JR. Hemodynamics in growing and stable cerebral aneurysms. *J Neurointerv Surg*. 2016;8(4):407-412. doi:10.1136/neurintsurg-2014-011339.

29. Meng H, Tutino VM, Xiang J, Siddiqui A. High WSS or low WSS? Complex interactions of hemodynamics with intracranial aneurysm initiation, growth, and rupture: toward a unifying hypothesis. *AJNR Am J Neuroradiol*. 2014;35(7):1254-1262.

doi:10.3174/ajnr.A3558.

30. Tsuji M, Ishikawa T, Ishida F, et al. Stagnation and complex flow in ruptured cerebral aneurysms: a possible association with hemostatic pattern. *J Neurosurg*. 2017;126(5):1566-1572. doi:10.3171/2016.3.JNS152264.

31. Sano T, Ishida F, Tsuji M, Furukawa K, Shimosaka S, Suzuki H. Hemodynamic Differences Between Ruptured and Unruptured Cerebral Aneurysms Simultaneously Existing in the Same Location: 2 Case Reports and Proposal of a Novel Parameter Oscillatory Velocity Index. *World Neurosurg*. 2017;98:868.e5-868.e10. doi:10.1016/J.WNEU.2016.12.047.

32. Fisher C, Rossmann JS. Effect of Non-Newtonian Behavior on Hemodynamics of Cerebral Aneurysms. *J Biomech Eng*. 2009;131(9):091004. doi:10.1115/1.3148470.

33. Maurits NM, Loots GE, Veldman AEP. The influence of vessel wall elasticity and peripheral resistance on the carotid artery flow wave form: A CFD model compared to in vivo ultrasound measurements. *J Biomech*. 2007;40(2):427-436. doi:10.1016/j.jbiomech.2005.12.008.

34. Marzo A, Singh P, Larrabide I, et al. Computational hemodynamics in cerebral aneurysms: the effects of modeled versus measured boundary conditions. *Ann Biomed Eng*.

2011;39(2):884-896. doi:10.1007/s10439-010-0187-z.

35. Russell JH, Kelson N, Barry M, Pearcy M, Fletcher DF, Winter CD. Computational fluid dynamic analysis of intracranial aneurysmal bleb formation. *Neurosurgery*. 2013;73(6):1061-8; discussion 1068-9. doi:10.1227/NEU.0000000000000137.

FIGURE LEGENDS

Fig. 1. Reconstruction of blood vessel shape using TOF-MRA data

(A) Original TOF-MRA image, (B) blood vessel model extracted from the TOF-MRA image, (C) STL (stereolithographic) mesh data of the blood vessel model, (D) signed-distance function representing blood vessel walls (the contour plots represent each iso-surface of the signed-distance function, whose magnitude is the distance from the blood vessel wall, while the sign of the function is determined in order to distinguish the solid phase [wall] from the fluid phase [blood]), and (E) time variation of inlet velocity during one cardiac cycle. The boundary condition at the wall in lattice Boltzmann simulations is given by making use of the distance function.

(TOF-MRA, time-of-flight magnetic resonance angiography.)

Fig. 2. Illustrative case: Case 1, 69-year-old woman, right IC-Pcom AN

The aneurysm measured 8.5 mm before growth (first row) and enlarged to 11.8 mm (second row) in 11 months. TOF-MRA imaging (first column) and analysis of flow dynamics, including the streamline (second column), wall shear stress (WSS, third and fourth columns), and oscillatory shear index (OSI, fifth column) were successfully obtained. WSS 2 shows a back view of WSS 1.

WSS was focally increased at the aneurysm wall (red arrow).

The change in WSS during one cardiac cycle is shown in the third and fourth rows (the third shows the status before aneurysm growth, and the fourth shows the status after growth). At the peak systolic phase, WSS was elevated at the focal aneurysmal sac before growth (red arrow heads), where the aneurysm would later enlarge.

(IC-Pcom AN, Internal carotid- posterior communicating artery aneurysm; TOF-MRA, time-of-flight magnetic resonance angiography.)

Fig. 3. Visual comparison of WSS analyzed by AN2WER (upper row) and by Hemoscope Ver. 1.5 (lower row) in three cases (one per column)

The areas with low WSS (blue) and relatively high WSS (green) on the aneurysm sacs were almost matched between the two methods. The color distributions at the parent artery were also similar between cases 2 and 3.

(CFD, computational fluid dynamics; WSS, wall shear stress)

Fig. 4. Results of the growing group

TOF-MRA images taken before and after aneurysm growth (first and second row, respectively). The peak values of WSS maps were recognized at the peak systolic phase (third row). WSS was focally increased on the walls of all aneurysms (red arrow). The mean values were 0.074, 0.106, 0.37, 0.13, 0.26, and 0.25 in cases 1 to 6, respectively. Fourth row: surface-rendered images demonstrating the calculated five points of peak WSS (white cross marks)

(first column, case 2; second column, case 3; third column case 4; fourth column, case 5; fifth column, case 6; sixth column, case 7).

WSS values are mean values at all five white cross marks in surface rendered images

(TOF-MRA, time-of-flight magnetic resonance angiography; WSS, wall shear stress)

Fig. 5. Results of the stable group

TOF-MRA images (first row), WSS map (second row) and surface-rendered images (third row) at the peak systolic phase of the stable aneurysms. In cases 1, 3 and 5, no apparent increases in WSS were recognized on the aneurysm sac. Obrained values were 0.0066, 0.045, and 0.0019, respectively. In the remaining three stable aneurysms (cases 2, 4, and 6), focal increases of WSS at the peak systolic phase (red arrow) were demonstrated. Obtained values were 0.487, 0.073, and

1 0.117, respectively (first column, case 1; second column, case 2; third column, case 3; fourth

2 column, case 4; fifth column, case 5; sixth column, case 6).

3 WSS values are the mean values at all five white cross marks in surface-rendered images

4 (TOF-MRA, time-of-flight magnetic resonance angiography; WSS, wall shear stress)

5

6 Fig. 6. Peak values of WSS on the focal aneurysm sac in both growing and stable aneurysms

7 The difference was statistically significant between the groups (* p <0.05).

8 (ANs, aneurysms)

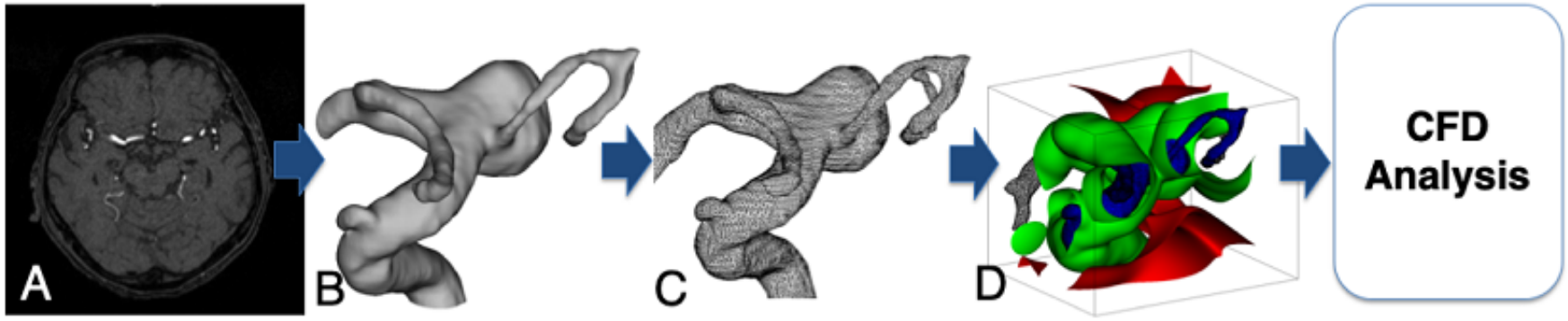

Dimensionless groups	
Reynolds number	200
Womersley number	2.5
Bingham number	0.1

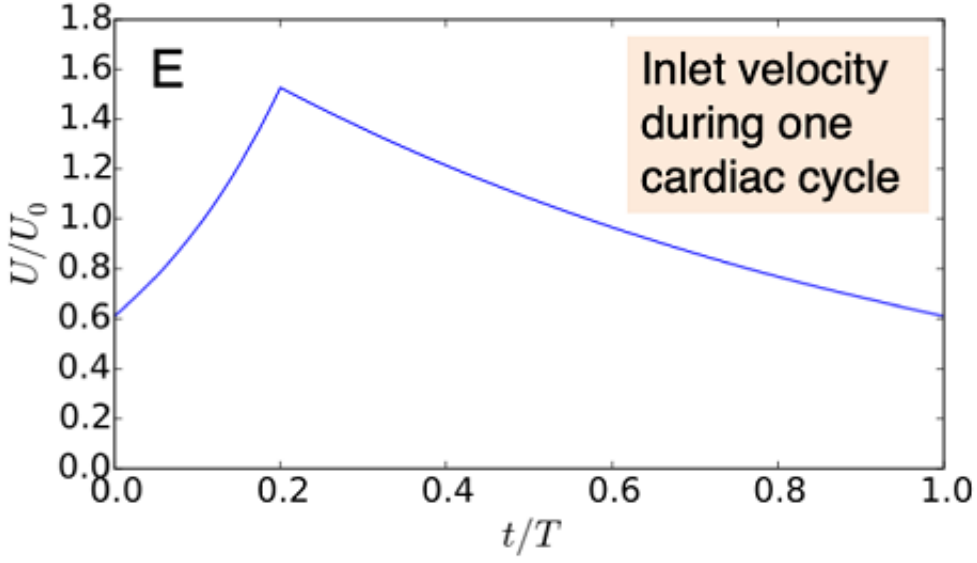

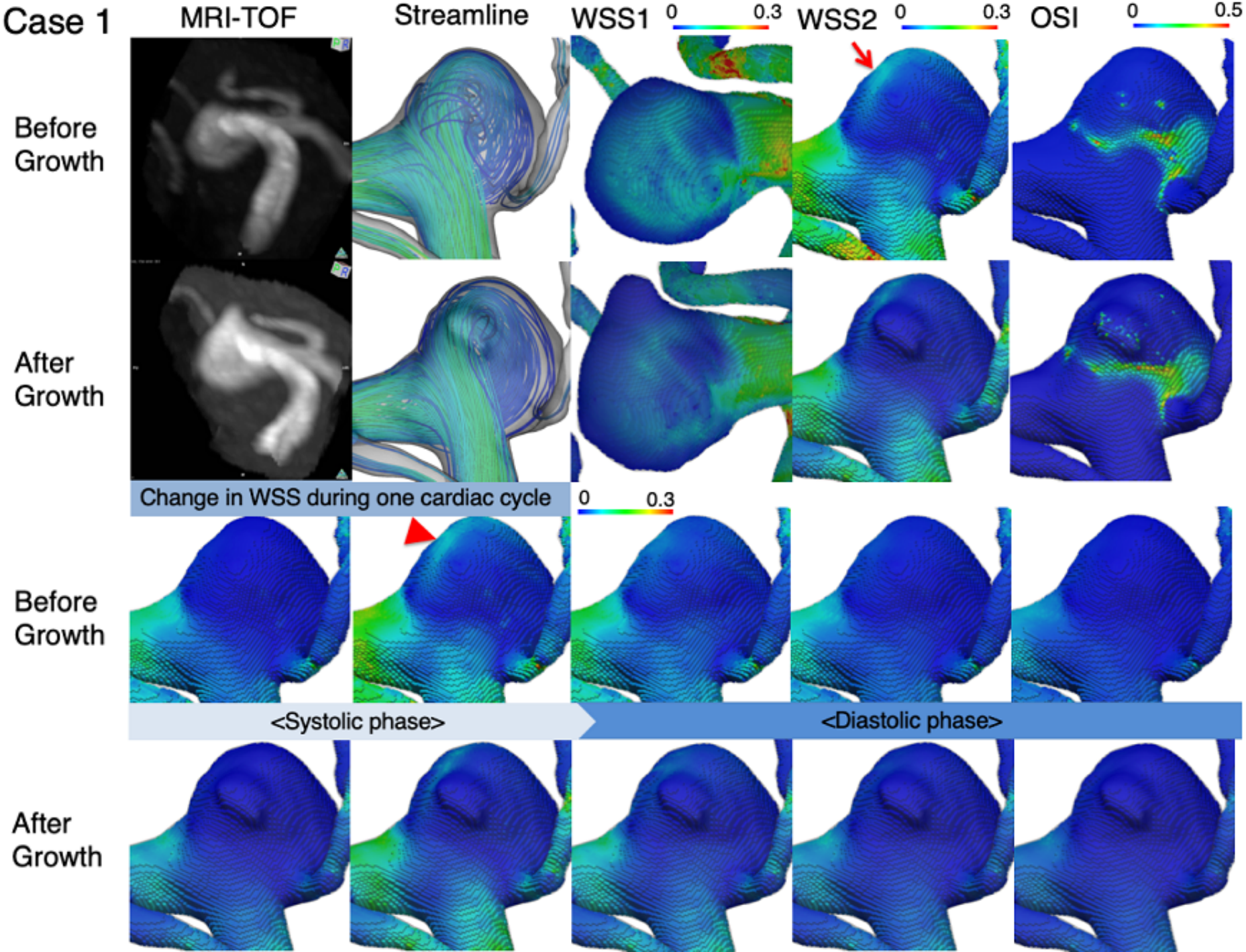
Case 1
MRI-TOF
Streamline
WSS1
0
0.3
WSS2
0
0.3
OSI
0
0.5
Before Growth
After Growth
Change in WSS during one cardiac cycle
0
0.3
Before Growth
<Systolic phase>
<Diastolic phase>
After Growth

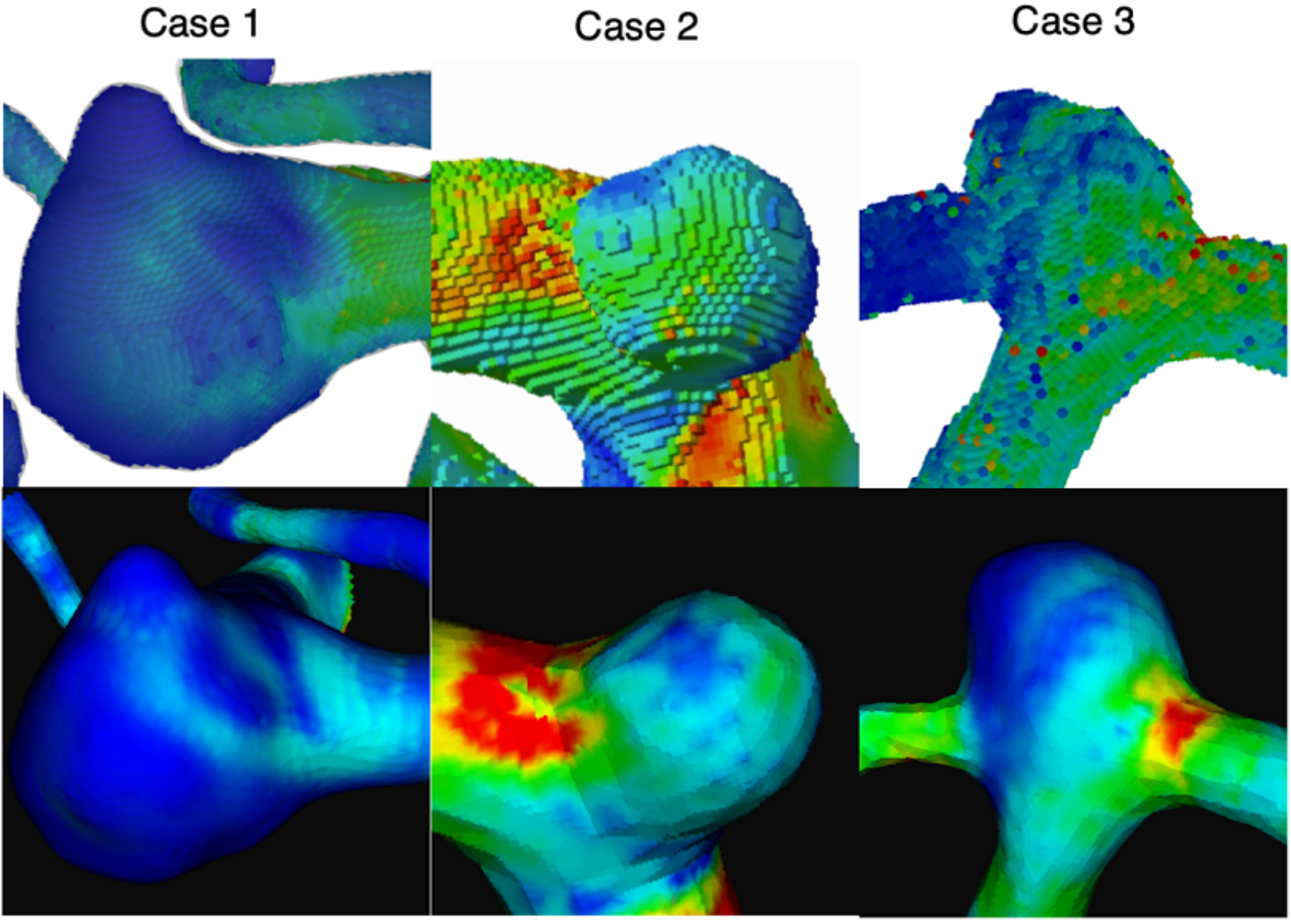
Case 1
Case 2
Case 3

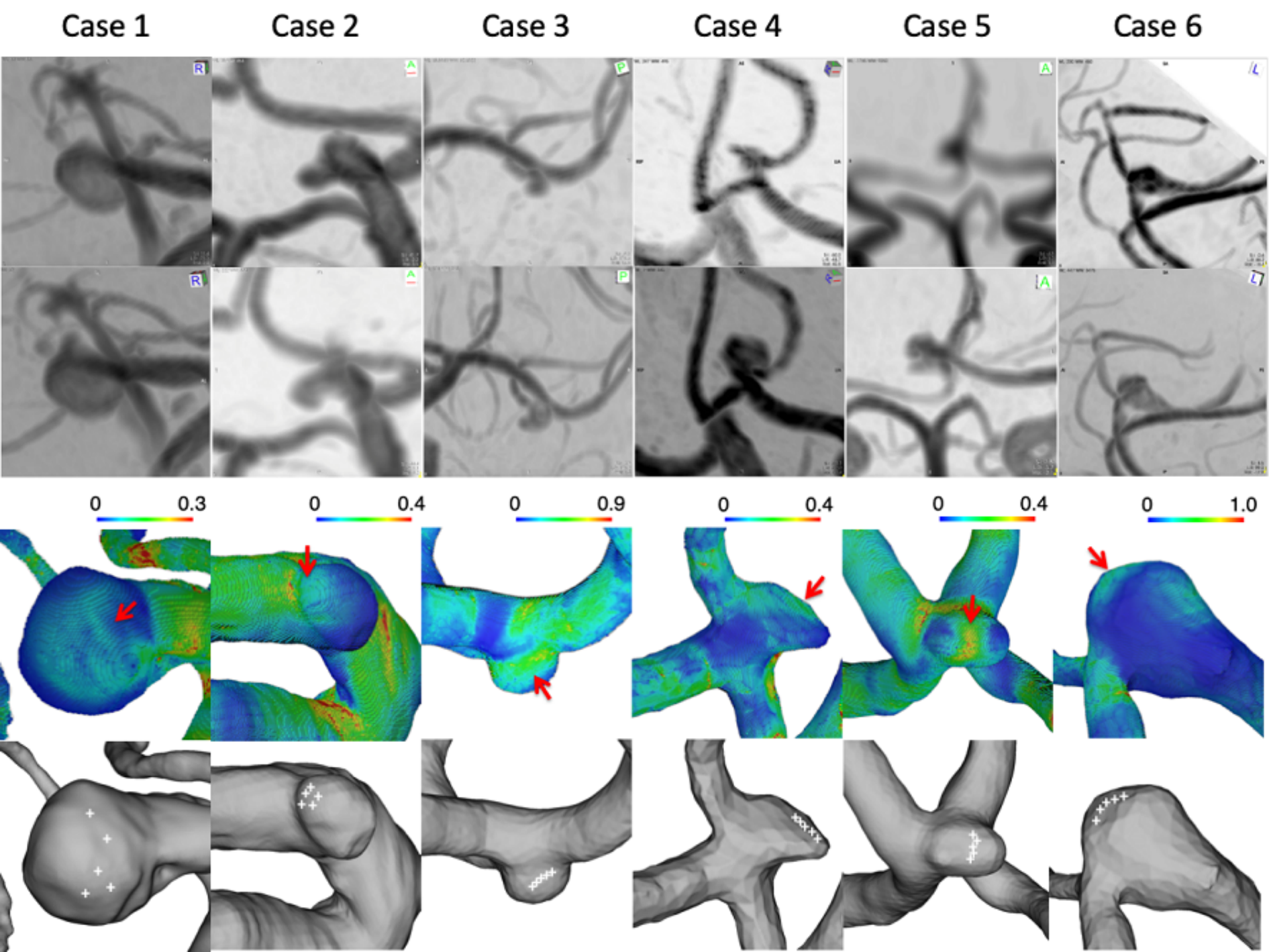
Case 1
Case 2
Case 3
Case 4
Case 5
Case 6
0
0.3
0
0.4
0
0.9
0
0.4
0
0.4
0
1.0

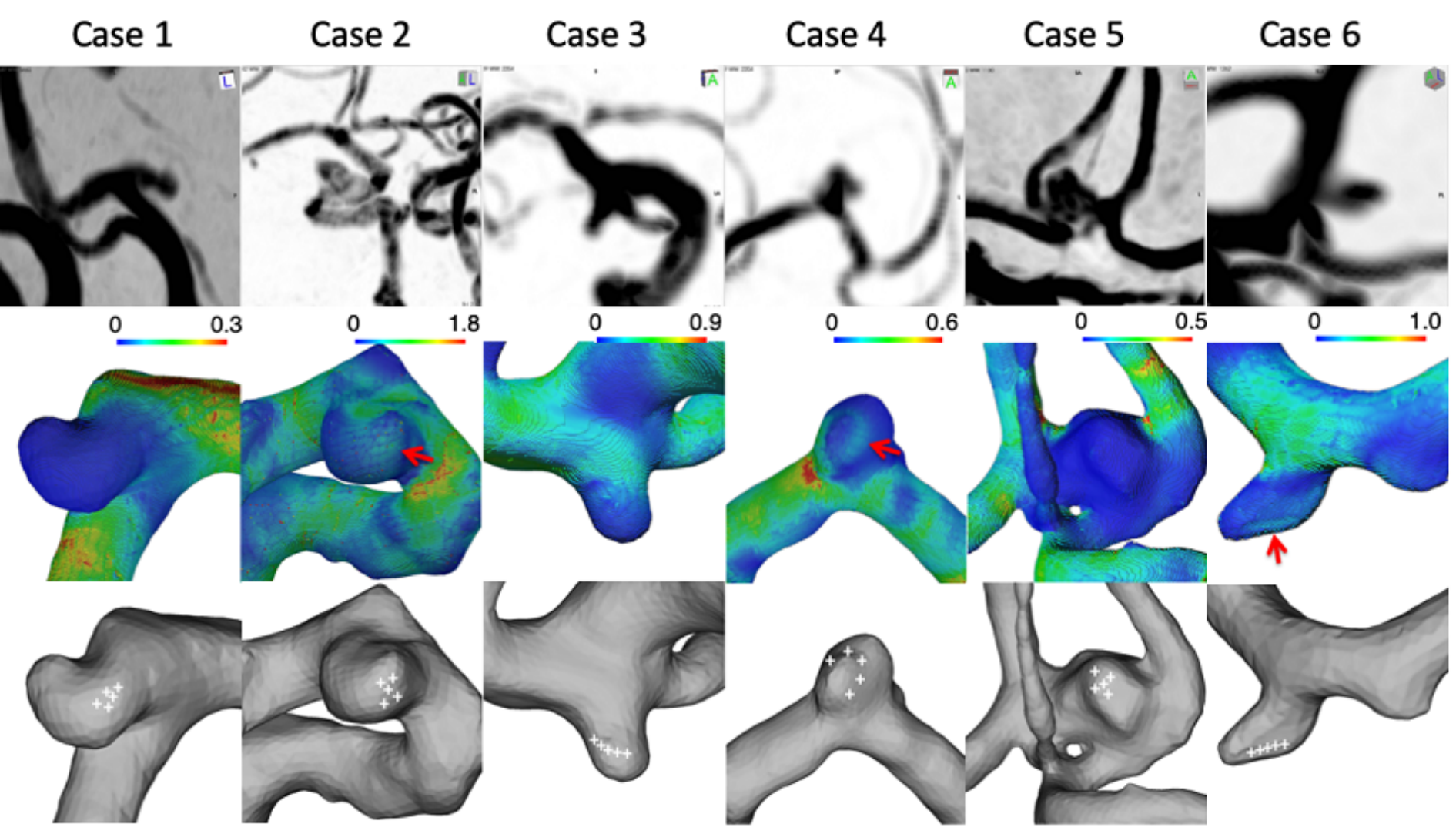
Case 1
Case 2
Case 3
Case 4
Case 5
Case 6
0
0.3
0
1.8
0
0.9
0
0.6
0
0.5
0
1.0

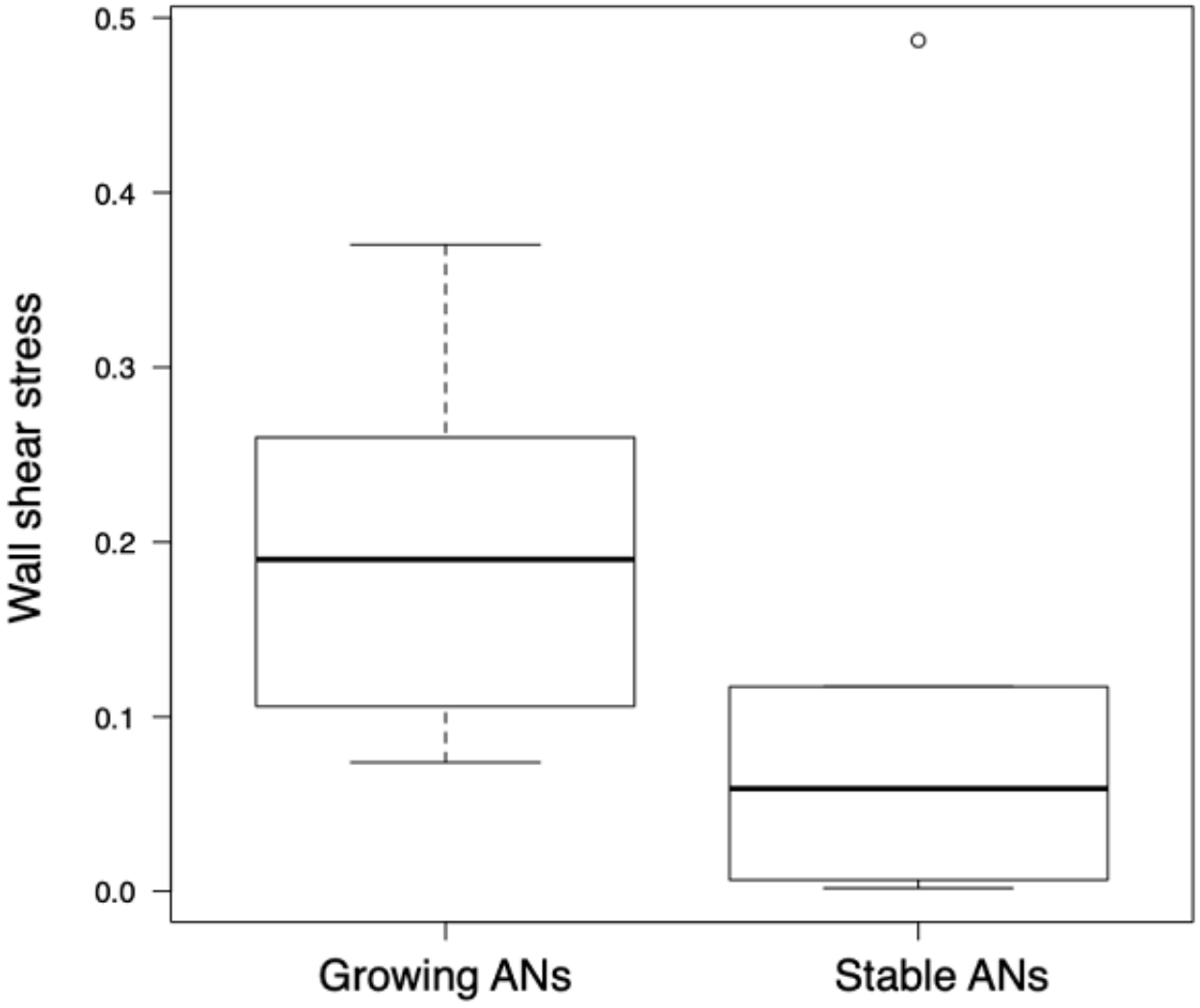
Wall shear stress
0.5
0.4
0.3
0.2
0.1
0.0
Growing ANs
Stable ANs

	Growing (n=6)	Stable (n=6)	p value
Mean age (years)	63.0±14.1	73.7±9.3	0.19
Men/women	1/5	1/5	1
Location			
IC	2 (33%)	3 (50%)	
Acom AN	2 (33%)	1 (17%)	
MCA	1 (17%)	1 (17%)	
VA-BA	0 (0%)	1 (17%)	
Distal ACA	1 (17%)	0	
F/U periods (month)	44.6	76.3	0.05
initial size	4.1±2.0	6.9±3.2	0.20
last size	6.1±2.6	–	